https://doi.org/10.5194/tc-2020-323
Preprint. Discussion started: 4 December 2020

The Cryosphere Discussions

High-resolution topography of the Antarctic Peninsula combining TanDEM-X DEM and REMA mosaic

Yuting Dong[1,2], Ji Zhao[3], Dana Floricioiu[2], Lukas Krieger[2], Thomas Fritz[2], Michael Eineder[2]

[1]School of Geography and Information Engineering, China University of Geosciences, Wuhan, China
[2]Remote Sensing Technology Institute (IMF), German Aerospace Center (DLR), Oberpfaffenhofen, Germany
[3] School of Computer Science, China University of Geosciences, Wuhan, China

Correspondence to: Ji Zhao (zhaoji@cug.edu.cn)

Abstract. The Antarctic Peninsula (AP) is one of the widely studied polar regions because of its high sensitivity to climate change and potential contribution to global sea level rise. Precise DEMs at high spatial resolution are highly demanded for investigating the complex glacier system of the AP at fine scale. However, the two most recent high-resolution DEMs covering the AP area, the 12-m TanDEM-X DEM (TDM DEM) from bistatic InSAR data acquired between 2013 and 2014 and the Reference Elevation Model of Antarctica mosaic (REMA mosaic) at 8 m posting derived from optical data acquired between 2009 and 2017 have specific individual limitations. The TDM DEM has the advantage of good data consistency and few data voids, but there exist residual height errors in the non-edited DEM version. The REMA mosaic on AP has high absolute vertical accuracy (about 1 m) but suffers from large areas with data voids and a larger time span within the images used to generate DEM. To generate a consistent, gapless and high-resolution (12 m) topography product of the AP, we combine the TDM DEM and REMA mosaic by detecting and correcting the height errors in TDM DEM through a novel path propagation algorithm and multi-scale height error correction method based on the accurately calibrated REMA mosaic data. The resulting DEM was evaluated with laser altimetry data and the Root Mean Square Error (RMSE) of the resulting DEM has been reduced by about 50% compared to the original TDM DEM. Remaining height errors especially due to phase unwrapping errors were successfully eliminated. The generated high-resolution DEM depicts the up-to-date topography of AP in detail and can be widely applied for glaciological studies at individual glaciers or at regional scale.

1 Introduction

Antarctic Peninsula (AP) glaciers (north of 70 ° S) have the potential to raise the global sea level by 69 ±5 mm (Huss and Farinotti, 2014) and their mass balance change is widely studied. Glaciers at the AP are sensitive to climate and oceanographic change and have undergone extensive changes in recent decades (Cook et al., 2005;Cook et al., 2014;Cook et al., 2016;Seehaus et al., 2018;Rott et al., 2018;Rignot et al., 2019;Dryak and Enderlin, 2020). AP is a complex mountainous coastal glacier system and the mass balance of the outlet glaciers is affected by climate and oceanographic forcing and also by the subglacial and surrounding topography (Cook et al., 2012). Digital Elevation Models (DEMs) are the digital representation of the topography and are fundamental data for investigating glacial features and to monitor glacier dynamics

https://doi.org/10.5194/tc-2020-323
Preprint. Discussion started: 4 December 2020

at individual glaciers or at regional scales, such as delineation of drainage basins (Cook et al., 2014;Huber et al., 2017;Krieger et al., 2020a), quantifying glacier mass balance with the mass budget method (Rignot et al., 2011b;Shepherd et al., 2018;Sutterley et al., 2014) or geodetic methods (Abdel Jaber et al., 2019;Krieger et al., 2020b;Rott et al., 2018;Helm et al., 2014), calculating ice velocity (Rignot et al., 2011a;Mouginot et al., 2012), or providing constraints for geodynamic and ice flow modelling (Cornford et al., 2015;Ritz et al., 2015).

The previously released DEMs of AP are mostly covering the whole Antarctic continent. They have been derived from satellite radar altimetry (Helm et al., 2014;Li et al., 2017;Slater et al., 2018), laser altimetry (DiMarzio et al., 2007), a combination of both radar and laser altimetry (Bamber et al., 2009;Griggs and Bamber, 2009), optical photogrammetry (ASTER GDEM Validation Team, 2009, 2011;Abrams et al., 2020;Howat et al., 2019), the combination of several sources of remote sensing and cartographic data (Liu et al., 2001;Fretwell et al., 2013) and Synthetic Aperture Radar (SAR) interferometry (German Aerospace Center DLR, 2018). In addition, regional DEMs of the marginal areas of the ice sheet have been generated from stereoscopic data (Korona et al., 2009). The parameters of the DEMs mentioned above can be found in Table S1 of the supplementary material.

By analysing all these available DEMs, it can be noted that the DEMs of AP have always suffered from large elevation uncertainty, coarse resolution, wide data voids or incomplete data coverage, which are caused by the complex mountainous terrain and cloudy weather of AP. To generate accurate surface topography data of AP, Cook et al. (2012) have created a DEM posted at 100 m by improving the ASTER GDEM datasets and smoothing the erroneous surface, but the 100-m grid size is still too coarse to analyse the glaciers' features and dynamics at fine scale. To meet the demand for high-resolution topography information, two DEM products were recently released: the 12-m global TanDEM-X DEM (TDM DEM) based on InSAR data acquired between 2013 and 2014 and the 8-m Reference Elevation Model of Antarctica mosaic (REMA mosaic) derived from optical data acquired between 2009 and 2017 (Howat et al., 2019). The TDM DEM is characterized by good data consistency and few data voids, but there are residual height errors in the non-edited version. The REMA mosaic has advantage in high absolute vertical accuracy (about 1 m) and absence of regional outliers, but suffers from a large amount of data voids and limited temporal consistency due of the relatively wide time span of images used to generate the DEM.

To obtain a consistent, gapless and precise DEM product at high spatial resolution of AP, we intend to create a high-resolution DEM of AP by combining the TDM DEM and REMA mosaic, the two up-to-date DEMs with similar posting. In this study, we propose a novel multi-scale height error correction algorithm to automatically eliminate the remaining height errors in the TDM DEM facilitated with the REMA mosaic data. Adjacent pixels with similar height deviations from the real surface elevation can be automatically detected and merged into a common region, and then corrected with an average height offset compensation value specific to each detected region. Since remaining height errors in the TDM DEM exist at different scales, the height offset correction is performed to gradually eliminate these errors from large to small scale. The height accuracy of the resulting DEM was validated with laser altimetry data to illustrate the effectiveness of the proposed algorithm.

https://doi.org/10.5194/tc-2020-323
Preprint. Discussion started: 4 December 2020

2 Experimental area and data

2.1 Experimental area

The Antarctic Peninsula (AP) between 63 °S and 70 °S (Figure 1), belonging to Graham Land is a long coastal area along the Weddell Sea on the east side and the Bellingshausen Sea on the west side. Based on the newest glacier inventory of AP of Cook et al. (2014) and Huber et al. (2017), there are 860 marine-terminating glaciers out of 1590 glacier basins. It has complex mountainous terrain with elevations rising steeply from sea level at the coast towards snow-covered flat plateaus located above 1500 m. The highest peaks are close to 3000 m a.s.l. The outlet glaciers and cirques lie at lower altitude and flow into ice shelves or terminate as grounded or floating tidewater glaciers. Their accumulation areas connect with the plateaus directly or through the escarpments with steep slopes.

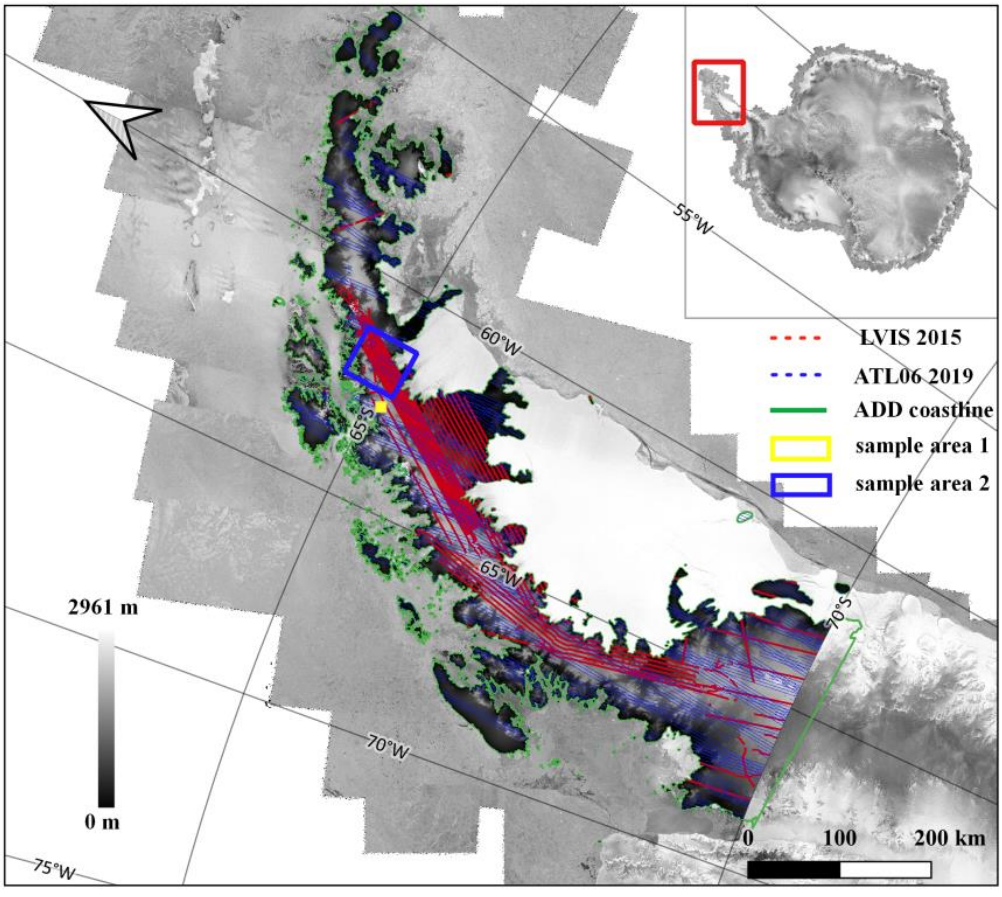

Figure 1. Experimental area and data coverage over Antarctic Peninsula. Red and blue dotted lines: the footprints of the LVIS 2015 and ATL06 2019 laser points, respectively. Green outline: the coastline mask from Antarctic Digital Database (ADD). Blue and yellow boxes: sample areas of the experimental results. Background: RADARSAT-1 Antarctic Mapping Project (RAMP) imagery mosaic (from Quantarctica).

https://doi.org/10.5194/tc-2020-323
Preprint. Discussion started: 4 December 2020

2.2 Experimental data

2.2.1 TanDEM-X DEM (TDM DEM)

The German TanDEM-X (TerraSAR-X add-on for Digital Elevation Measurements) mission is a bistatic SAR interferometer built by two almost identical satellites (TerraSAR-X and TanDEM-X) flying in close formation (Krieger et al., 2007;Krieger et al., 2013). The advantage of the single-pass SAR interferometer is to acquire highly coherent cross-track interferograms, which are not affected by temporal decorrelation and atmospheric phase delay. Besides, the TDM DEM is unaffected by the cloud cover or varying solar illumination conditions, which is the main reason for the completeness of TDM DEM. The primary objective of the TanDEM-X mission was the generation of a worldwide, consistent, timely, and high precision DEM as the basis for a wide range of scientific research. The resulting main product, the TDM DEM has a nominal pixel spacing in latitude direction of 0.4 arcsecond corresponding to approximately 12 m at the equator, a relative vertical accuracy of 2 m (slope < 20%) and an absolute vertical accuracy of 10 m (Rizzoli et al., 2017a). The TDM DEM is also available with a pixel spacing of 1 arcsecond and 3 arcseconds (Wessel, 2016), but in our study over the AP, we focus on the nominal product at about 12 m posting size. The elevation values represent the ellipsoidal heights relative to the WGS84 ellipsoid in the geographic coordinate system.

The bistatic InSAR data used for generating TDM DEM over Antarctica were acquired during two dedicated campaigns lasting from April to November of 2013 and 2014. The concentration of acquisition time over Antarctica reduces the temporal changes of the terrain surface and thus guarantees the consistency of the TDM DEM product. The TanDEM-X mission has acquired multi-coverage of Antarctica from different orbital directions and height ambiguities in order to compensate for geometric distortions (Gruber et al., 2016) and improve phase unwrapping with the dual-baseline phase unwrapping algorithm (Lachaise et al., 2017). However, due to the complicated mountainous terrain condition of AP, there still exist height errors caused by phase unwrapping error and geometric distortions in the non-edited TDM DEM, which contaminates the height measurement accuracy of TDM DEM. Besides, the elevation offset and horizontal shift because of calibration error will also propagate into the final DEM product due to the mosaic processing.

2.2.2 The Reference Elevation Model of Antarctica (REMA) mosaic

The REMA DEM was generated from stereo photogrammetry with high-resolution optical, commercial satellite imagery and covers nearly 95% of the entire Antarctica. Unlike other common stereo-capable imagers such as Advanced Spaceborne Thermal Emission and Reflection Radiometer (ASTER), the optical imagery used for generating REMA is of high spatial and radiometric resolution, which ensures accurate measurements over low-contrast ice sheet surface (Howat et al., 2019).

The REMA mosaic at 8 m resolution used in this paper was provided in 100 × 100 km^2 tiles and mosaicked from the individual time-stamped DEM strips which were quality-controlled and vertically registered (Howat et al., 2019). The absolute vertical accuracy of the REMA strips and mosaic products is less than 1 m based on validation with data acquired by three NASA Operation IceBridge (OIB) airborne lidar instruments: the Airborne Topographic Mapper (ATM), the Land,

https://doi.org/10.5194/tc-2020-323
Preprint. Discussion started: 4 December 2020

Vegetation and Ice Sensor (LVIS), and the ICECAP laser altimeter system (Howat et al., 2019). Considering the data acquisition efficiency and the effects of cloud cover and varying illumination, the limitations of the REMA mosaic are that the time span of stereo image acquisition to generate the REMA mosaic lasted for 9 years from 2009 to 2017 and there are approximate 8% data voids in the final DEM mosaic at AP based on our statistics.

The REMA mosaic is referenced to WGS 84 ellipsoid and in polar stereographic projection with a central meridian of 0 ° and standard latitude of -71 °S. For the present paper, we converted the REMA mosaic to the geographic coordinate system with the same grid size as the TDM DEM.

2.2.3 Laser altimetry data

In order to evaluate the height accuracy of the TDM DEM before and after automatic correction, we use the airborne laser altimetry data over Antarctica acquired by NASA OIB. We selected the LVIS Level 2 geocoded elevation product acquired in 2015 for its dense coverage in the central part of AP (Figure 1). The vertical height accuracy of LVIS is about 0.1 m and the footprint size is about 20–25 m (Hofton et al., 2008).

To obtain a complete evaluation of the whole experimental area, we also use the evenly distributed Level 3A geocoded land ice height data set ATL06 acquired in austral winter of 2019 by the Advanced Topographic Laser Altimeter System (ATLAS) instrument of the ICESat-2 satellite mission. The ATL06 footprint is about 17 m in diameter and the surface height measurement accuracy is better than 0.1 m (Brunt et al., 2019). The coverage of ATL06 data is shown in Figure 1. For simplicity of the presentation, the two laser altimetry datasets used as validation data are abbreviated as LVIS 2015 and ATL06 2019.

2.2.4 Coastline mask

In order to improve the calculation efficiency, we use the coastline mask from Antarctic Digital Database (ADD) (https://add.data.bas.ac.uk/, last access: 13 February 2020) which is marked by the green outline in Figure 1. The current version 7.1 was last updated in August 2019. We have visually checked the agreement between the ADD coastline product and hillshade map of TDM DEM at AP and found most of the glacier fronts are contained within or agree with the ADD coastline.

3 Methodology

We propose a novel method to detect and correct the residual height errors in the 12 m TDM DEM facilitated by the REMA 8 m mosaic tiles. The detailed methodologies are organized in four modules (Figure 2). Firstly, we analysed the characteristics of the residual multi-scale height errors in the TDM DEM with the REMA mosaic as ground truth. Secondly, we developed a path propagation algorithm to automatically detect the erroneous regions with height offset based on height error scales and spatial adjacency. Thirdly, instead of replacing the erroneous height values with the corresponding REMA

https://doi.org/10.5194/tc-2020-323
Preprint. Discussion started: 4 December 2020

mosaic, we selected stable points from the buffer zone of the erroneous region in TDM DEM to fit a reference height surface and then calculate the compensation offset to the fitted height surface. Fourth, the above detection and correction procedure is iteratively performed to correct multi-scale height errors. Details of each module are given in the following sections.

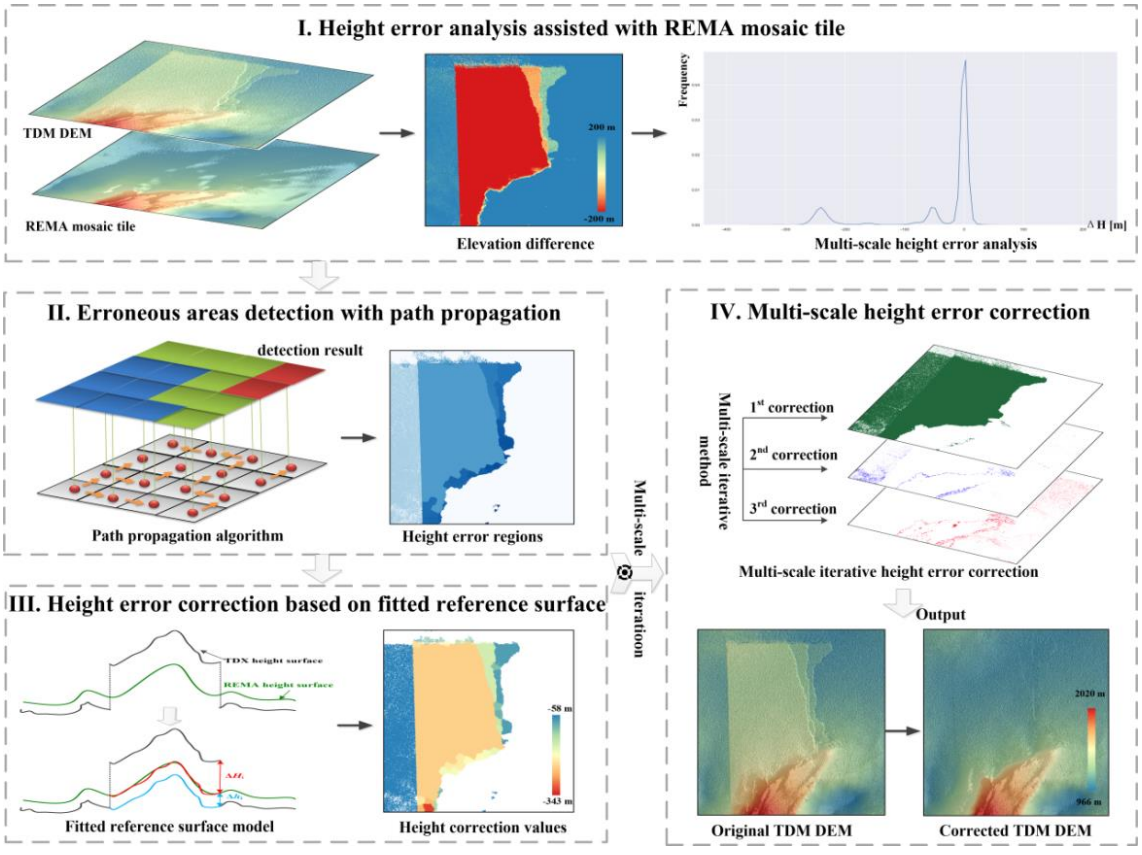

Figure 2. The framework of TDM DEM correction with REMA mosaic tiles organized in modules I to IV.

3.1 TDM DEM height error analysis assisted with REMA mosaic

The remaining height errors in the TDM DEM include the random height error introduced from the phase noise and the systematic height errors caused by the baseline calibration error, geometric distortions such as layover and shadow, and phase unwrapping (PU) errors. Details on each of these height errors are given below.

(1) Random height error

The random or theoretical height error of TDM DEM is linearly related to the interferometric phase error that depends on the coherence and baseline geometry and slightly increases from near to far range (Rizzoli et al., 2012;Rizzoli et al., 2017a). A height error map (HEM) is accompanying each TDM DEM tile representing a combined estimate of the corresponding random height error σ_{ran} from the interferometric coherence and geometrical considerations (Wessel, 2016). The TDM DEM is generated from weighted average of DEMs acquired from multiple coverages to reduce the random height error. Based on

https://doi.org/10.5194/tc-2020-323
Preprint. Discussion started: 4 December 2020

the specification of the TDM DEM, the relative height accuracy which accounts for random height error only is less than 2 m at flat terrain (< 20% local slope), and less than 4 m at mountainous terrain (> 20% local slope) estimated at a 90% confidence level (Gruber et al., 2016). However, this relative height accuracy specification of the TDM DEM is a global statistic and local performance could be degraded, due to the presence of confined local outliers (Rizzoli et al., 2017a). AP is a mountainous area with snow and ice coverage and the volume scattering decorrelation of the snow can increase the random phase noise locally.

(2) Height error from baseline calibration

The TDM DEM has gone through a sophisticated calibration process to improve the baseline accuracy, including instrument and baseline calibration (Gonzalez et al., 2012). The correction of residual offsets and tilts in azimuth and range is performed by means of a least-squares block adjustment with ICESat laser altimetry data (Gruber et al., 2012). The final baseline accuracy is in the order of 1 mm for a ground extension of about 30 km × 50 km, which corresponds to a vertical offset on the order of 1 m (Rizzoli et al., 2017a). A vertical offset is always accompanied by a tilt and a shift in range direction for DEM scenes. When combining the DEM scenes together into the final mosaic, the vertical offsets and horizontal shifts are likely to cause elevation bias or block-shaped height anomaly when there are residual phase unwrapping errors.

(3) Height error from geometric distortions

At the high-relief terrain, the DEM quality is reduced due to the geometric distortions such as the layover or shadow. The erroneous regions affected by the geometric distortions can be data voids or outliers. This kind of height error is usually compensated with the fusion of ascending and descending DEM acquisitions. As for the TanDEM-X mission, the land mass was mapped at least twice with complementary imaging geometries and the acquired DEMs were screened and the non-discrepant data were grouped and then weighted averaged to generate the final TDM DEM, which can effectively fill in most data gaps caused by layover or shadow (Gruber et al., 2016). The remaining height error due to geometric distortions is small in spatial size and sparsely distributed over the steep slopes oriented towards the radar or away from it.

(4) Height error from phase unwrapping error

The phase unwrapping is a crucial step in interferometric applications hence also in the surface elevation retrieval. It is very difficult to achieve an error-free phase unwrapping at AP because the complex mountainous terrain is prone to cause dense fringes and phase jumps. PU errors typically correspond to height inconsistencies in the order of an integer multiple of the height of ambiguity (HoA). The HoA is the height that corresponds to one phase cycle after phase-to-height-conversion and is typically in the range of 30 to 80 m for most of the twin satellites baseline configurations during the nominal TanDEM-X acquisitions.

For TDM raw DEMs, Gruber et al. (2016) estimated the minimum height inconsistency $dp_{PUthres}$ introduced by phase unwrapping errors as $dp_{PUthres}$ =0.75*min(|H_OA|)-4 [m] considering the random height error (empirically set as 0.25*min(|H_OA|) [m]) and the possible residual calibration inaccuracies (within 4 m). In our study, we detect the residual height errors in TDM global DEM through calculating height difference map ΔH with REMA mosaic. The minimum height

https://doi.org/10.5194/tc-2020-323
Preprint. Discussion started: 4 December 2020

discrepancy $\Delta H_{PUthres}$ due to phase unwrapping errors in TDM DEM is empirically adjusted to Eq. (1). The first item in the right part of Eq. (1) is reduced to 0.6*min(|H_OA|) [m] because the AP is a mountainous area with snow and ice cover which causes higher random height noise for both TDM DEM and REMA mosaic. $\Delta H_{PUthres}$ is then reduced by 1 m considering the calibration error of TDM global DEM is at about 1 m (Rizzoli et al., 2017a). Since the minimum height ambiguity of the TanDEM-X mission is about 30 m, the minimum height inconsistency $dp_{PUthres}$ is approximately 17 m based on Eq. (1).

$$\Delta H_{PUthres} = 0.6 \cdot \min\left(\left|H_O A\right|\right) - 1 \quad (1)$$

From the above analysis, it can be seen that the remaining height errors in TDM DEM causing large inconsistencies are mainly introduced by the systematic height errors especially the phase unwrapping error. We propose to detect and correct the remaining systematic height errors in the TDM DEM with the REMA mosaic as reference DEM.

Figure 3a shows a sample area with phase unwrapping error in TDM DEM, which is also visible as an elevation jump in the TDM DEM height profile crossing the boundary of the inconsistent region (Figure 3b) as well as a large discrepancy in the height difference map between TDM DEM and REMA mosaic (blue region in Figure 3c). In the height difference histogram (Figure 3d), the remaining height error can be seen as side lobes adjoining the main lobe near zero. This abnormal elevation jump distinguishes the phase unwrapping errors from the temporal change in elevation or penetration depth which are transitional changes with a certain trend. In other words, the height error in TDM DEM caused by the phase unwrapping error is characterized by local height discrepancies with abrupt elevation jumps at the boundary where they occur. Height error caused by the geometric distortions such as layover or shadow also exists at rugged terrain. It has more variations in smaller spatial size compared to the phase unwrapping error. In the following sections (Section 3.2 to Section 3.4), we are using the characteristics of the remaining height errors to detect and correct these large discrepancies present in the TDM DEM.

https://doi.org/10.5194/tc-2020-323
Preprint. Discussion started: 4 December 2020

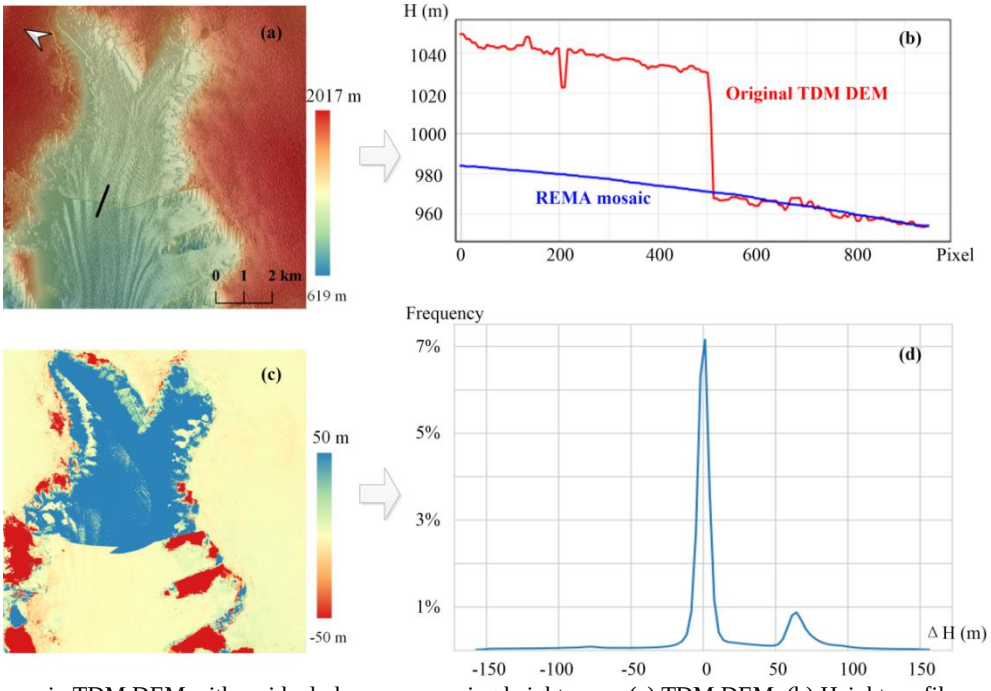

Figure 3. Sample area in TDM DEM with residual phase unwrapping height error. (a) TDM DEM. (b) Height profile corresponding to the black line in (a). (c) Height difference map between TDM DEM and REMA mosaic. (d) Histogram of the height difference map.

3.2 Erroneous areas detection with path propagation algorithm

The automatic detection of the areas with height errors from the height difference map between the TDM DEM and REMA mosaic is performed with a novel path propagation algorithm where neighboring pixels with similar local height offset value are detected and merged into one region as illustrated in Figure 4. The elevation difference value in meters for each pixel used as input is shown in Figure 4a. The pixels can be divided into background and target pixels based on their corresponding height difference values. The background pixels (in grey in Figure 4b and 4c) have height differences below a threshold value and will not be corrected in the following process. The remaining pixels are regarded as target pixels to be processed (light orange pixels in Figure 4b). The main task is to merge spatially adjacent target pixels with similar local height offsets into common regions. Then each of these regions can be corrected individually by the compensation value of the corresponding region. With the path propagation method, the target pixels will search their 4- or 8-neighborhood direction for homogeneous pixels. For simplicity of explanation in Figure 4b only the 4-neighborhood search is shown. The similarity criterion between the adjacent target pixels i, j is the absolute difference of their elevations (H):

$$\left|H_i - H_{j\in N_i}\right| \le T_{\Delta H} \tag{2}$$

Where $T_{\Delta H}$ is the given threshold and N_i represents the neighborhood of pixel i. If the similarity criteria in Eq. (2) is fulfilled, the corresponding neighboring target pixels will be merged into the same region.

https://doi.org/10.5194/tc-2020-323
Preprint. Discussion started: 4 December 2020

The new-added target pixels will continue searching their neighboring target pixels. To correctly compensate for the mean height offset of the erroneous region, it is important to detect the regions with homogeneous offset accurately. The existence of background pixels improves the calculation efficiency and most importantly cuts off the propagation path of target pixels. Furthermore, it is very important to properly inhibit the propagation path of target pixels not only with the background pixels but also based on the dissimilarity between the neighboring target pixels. In our example we set $T_{\Delta H}$=7 m for the neighboring pixels and pixels along the propagation path (marked with green arrows in Figure 4b) can be merged into one region. The propagation path stops at pixels with absolute elevation difference larger than $T_{\Delta H}$ as well as at the background pixels. Finally, the target pixels are merged into two separate regions according to the similarity of the height offsets (Figure 4c).

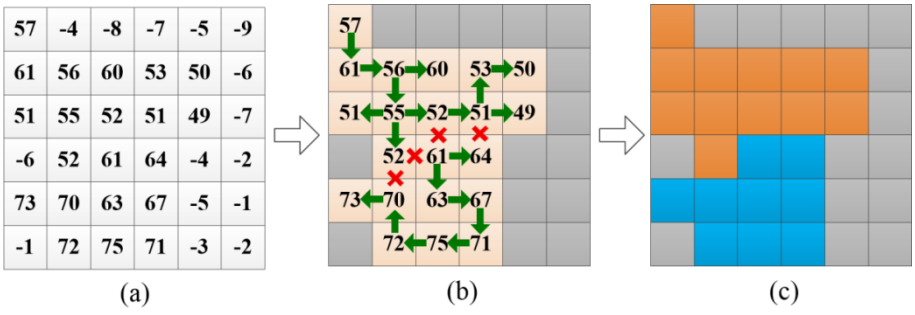

Figure 4. Erroneous areas detection with path propagation algorithm. (a) TDM DEM – REMA elevation difference values in meter, (b) Elevation jump detection with path propagation. Green arrows and red crosses respectively represent the adjacent pixels which can and can not be merged along the propagation path. Grey: background pixels. (c) Resulting automatically merged regions in orange and blue with mean elevation difference of 53.9 m and 68.4 m, respectively.

3.3 Height errors correction based on fitted reference surface

After merging the targeting pixels with similar local height offsets into regions, the height error correction of TDM DEM based on the REMA mosaic taken as reference is performed for each of these regions. Taking the differences due to the SAR signal penetration depth into snow and firn and to possible temporal elevation changes between the TDM DEM and REMA mosaic into consideration, we do not just correct the TDM DEM to the reference height surface of REMA mosaic directly. Instead, we create a buffer zone around each corrected region. Stable points whose height difference with REMA mosaic is less than a given threshold value are extracted from the buffer zone. The average height surface fitted from these selected stable points is used as a reference height surface for height offset correction. As shown in Figure 5 the correction height value $\Delta\hat{H}_{corr,i}$ for each region i can be calculated as the sum of the average height difference between REMA mosaic and TDM DEM, ΔH_i and the mean height difference of selected stable points inside the buffer zone, Δh_i:

$$\Delta\hat{H}_{corr,i} = \Delta H_i + \Delta h_i \quad (3)$$

https://doi.org/10.5194/tc-2020-323
Preprint. Discussion started: 4 December 2020

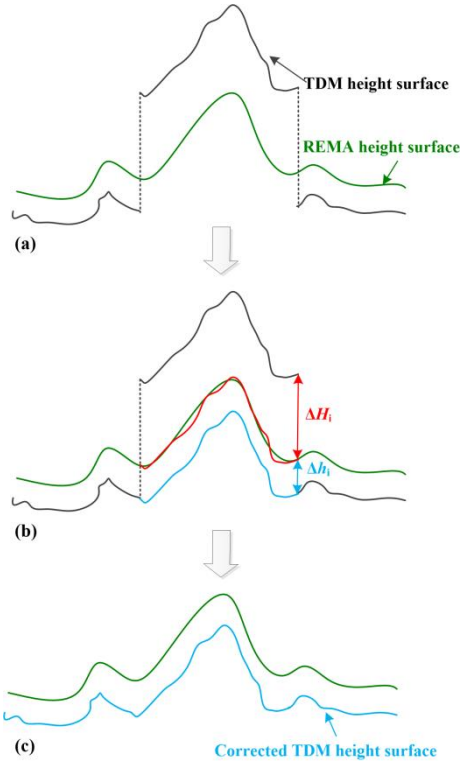

Figure 5. Local height offset correction procedure. (a) Erroneous elevation jump of TDM DEM and the REMA surface height, (b) Correction of the jump with fitted height surface as in Eq. (3). Red: corrected height surface with mean offset, Blue: corrected height surface with additional fitted height surface. (c) Finally corrected TDM DEM.

3.4 Multi-scale corrections of height errors in TDM DEM

Since the residual height errors in TDM DEM may have a wide range of values, the histogram of the TDM DEM height errors (quantified as differences to REMA mosaic elevations) usually has several side lobes adjoining the main zero centered lobe as illustrated in the first module of Figure 1 and Figure 3d. Actually it is likely to find additional smaller side lobes inside the large side lobes. Consequently, the segmentation results of the erroneous regions from the path propagation algorithm may also contain pixels with height offsets at different scale. Thus, the inhomogeneous region can not be accurately corrected just with the mean offset value.

To compensate the remaining height errors in the TDM DEM more accurately, we propose to adopt a multi-scale correction method to gradually correct the height errors from large to medium and small-scale. As described in Section 3.2 the path propagation algorithm is only performed among pixels with height difference larger than a certain threshold, all other pixels being labeled as background pixels. For each correction, the background pixels which do not need to be corrected are set based on the threshold that determines different height error scales. In order to achieve accurate segmentation results of the height inconsistency regions, the path propagation should be effectively cut off at the boundaries between different erroneous regions. The large-scale height error has a clear boundary in the height difference map and can

https://doi.org/10.5194/tc-2020-323
Preprint. Discussion started: 4 December 2020

be easier detected and corrected. Therefore, the multi-scale correction method starts with the large-scale height error by setting an empirically determined threshold on the TDM DEM to REMA mosaic height difference. In this step all the pixels with height difference less than the threshold are marked as background and no correction is applied. After this first iteration of large-scale height error correction, the number of background and stable points needed for the following medium-scale or small-scale correction steps is increasing and the propagation path for target pixels merging can be well restricted and cut off. Hence, the homogeneity degree of the merged regions in terms of height errors is increased accordingly. Similarly, the medium- or small-scale height errors are successively corrected to obtain a high precision corrected DEM. Examples of how the multiscale correction is applied are shown in Section 5.2.

4 Experiments

In order to test the effectiveness of the proposed algorithm at different spatial scales, we applied our methodology on a series of sample areas. Their spatial extension is increasing from local, about 11×11 km^2 large area, to glacier scale (yellow and blue rectangles in Figure 1) and finally cover the entire Antarctic Peninsula. The resulting corrections were validated with the laser altimetry data sets LVIS 2015 and ATL06 2019 described in Section 2.2.3.

4.1 Experimental results at local area

When comparing the original TDM DEM and the corresponding REMA mosaic (Figure 6a and Figure 6b, respectively) elevation surface offsets with boundaries caused by phase unwrapping and DEM calibration errors are visible in the TDM DEM as well as in the height difference map (Figure 6c). The voids visible in the REMA mosaic 8 m tile (Fig 6b) were filled with the oversampled 100 m-posting REMA mosaic tiles leading to a gapless elevation difference map. We applied the proposed multi-scale correction algorithm to calculate the correction values (Figure 6d) based on the elevation difference map (Figure 6c). Finally, the corrected TDM DEM (Figure 6e) results in a smooth height surface after successfully removing the elevation offsets. The height difference map between the corrected TDM DEM and REMA mosaic (Figure 6f) shows a more consistent trend around zero with height difference range reducing from ± 200 m (Figure 6c) to ± 50 m.

The DEM height error at each LVIS and ATL06 point (Fig 6a) was calculated as the height difference between laser point height and the height of the geographically closest point in the DEM (Table 1). We divided the total height range of the sample area into the sub-ranges 1000–1500 m and 1500–2000 m. Absolute height differences larger than 300 m were eliminated as outliers. For REMA mosaic, the RMSE inside the height range 1500–2000 m is less than 2 m and the 90% quantile is no more than 4 m for both LVIS 2015 and ATL06 datasets, indicating that the REMA mosaic is high-precision and qualified as ground truth for TDM DEM height errors correction. For the corrected TDM DEM, the absolute mean height error and RMSE reduce considerably compared to the original TDM DEM. For height range 1500–2000 m, the absolute mean height error has decreased from larger than 45 m to less than 2 m and the RMSE has decreased from larger than 75 m to less than 5 m.

https://doi.org/10.5194/tc-2020-323
Preprint. Discussion started: 4 December 2020

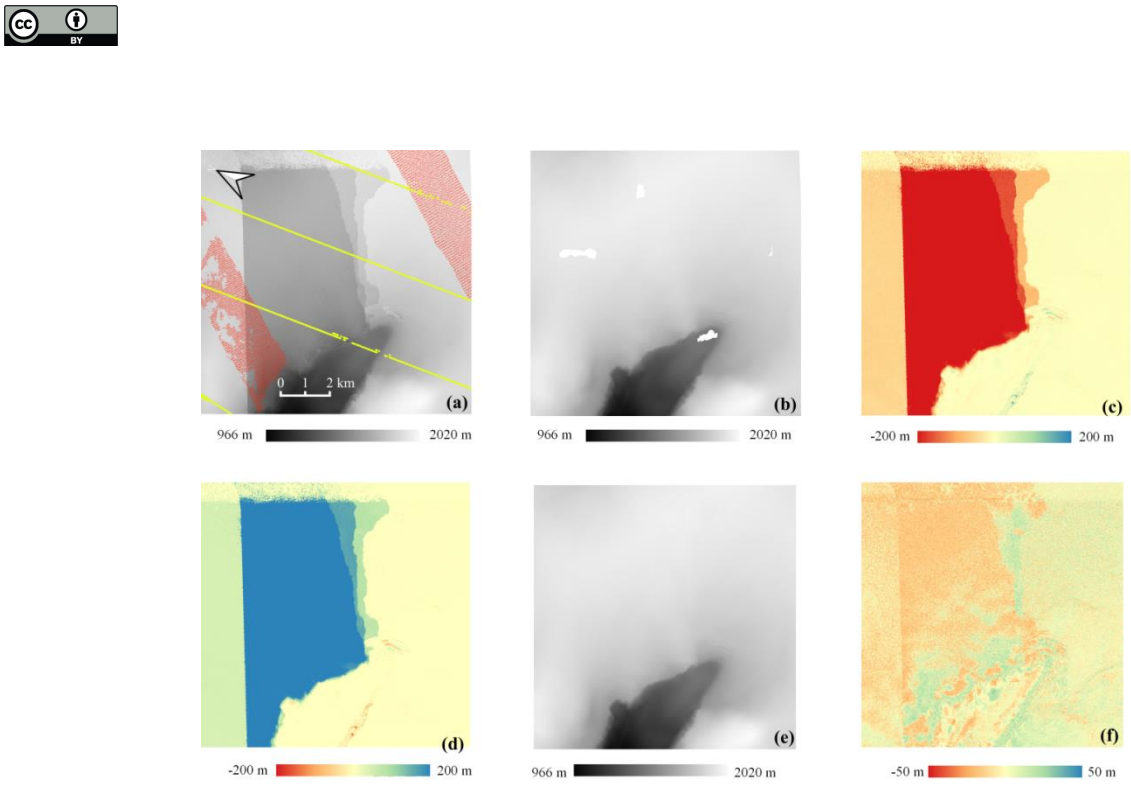

Figure 6. Experimental results on a local 11 × 11 km^2 sample area. (a) original TDM DEM. Red and yellow: the footprints of LVIS 2015 and ATL06 2019. (b) original REMA mosaic elevations with unfilled voids. (c) elevation difference between TDM DEM and REMA mosaic. Height differences calculated as TDM DEM minus REMA mosaic. (d) correction map as obtained with Eq. (3). (e) corrected TDM DEM. (f) residual elevation difference between the corrected TDM DEM and REMA mosaic.

Table 1. Statistics of DEM height differences between the laser points and the REMA mosaic, original and corrected TDM DEMs over the local sample area in Figure 6. All height units are in meters. Height differences calculated as DEM elevation minus laser height.

		Height range	Num. of points	Mean	RMSE	90% quantile
LVIS 2015	REMA mosaic	1000-1500	20	5.1	3.9	9.2
		1500-2000	43513	2.1	1.6	4.0
	Original TDM DEM	1000-1500	3877	-222.8	22.9	-205.0
		1500-2000	39646	-48.7	78.5	6.0
	Corrected TDM DEM	1000-1500	20	6.0	3.3	10.0
		1500-2000	43535	1.6	4.7	8.0
ATL06 2019	REMA mosaic	1000-1500	49	0.9	1.9	3.0
		1500-2000	1607	0.8	1.3	2.0
	Original TDM DEM	1000-1500	96	-109.4	110.7	2.0
		1500-2000	1560	-86.6	98.0	3.0
	Corrected TDM DEM	1000-1500	49	-1.5	3.5	3.0
		1500-2000	1607	-1.3	4.6	5.0

https://doi.org/10.5194/tc-2020-323
Preprint. Discussion started: 4 December 2020

4.2 Experimental results on Hektoria and Green Glaciers

For testing of our method at glacier scale, we selected an area of about 55 km × 60 km covering the Hektoria and Green (HG) glaciers, two adjacent outlets on the Eastern AP. The height difference map between original TDM DEM and the void filled REMA mosaic (Figure 7c) clearly shows erroneous regions with height errors of tens of meters in the TDM DEM. After applying the same methodology demonstrated for the local experimental area (Section 4.1) the erroneous regions are considerably reduced as revealed by the elevation difference map between the corrected TDM DEM and REMA mosaic (Figure 7f).

The laser altimetry point measurements (coverage shown in Figure 7a) were used to validate our correction over HG area. We divided the elevation range of the scene (18 m to 2150 m) into 5 intervals for which we calculated the corresponding statistics of the height differences between the TDM and laser elevations (Table 2). Same as in Section 4.1, the DEM pixels with absolute height differences larger than 300 m were eliminated. The variable topography of the elevations intervals influence the RMSE of DEMs. Above 1500 m on the flat firn plateaus the RMSE is the smallest. Below 1000 m a.s.l. where the outlet glaciers of AP are mainly located the RMSE is noticeably larger. This may be explained by the fact that HG are among the fastest changing outlet glaciers on AP in terms of surface elevation and frontal advance (Rott et al., 2018) and the different acquisition years of the laser altimetry data and the DEMs. The steep escarpment, dropping abruptly about 500 m in elevation from 1500 to 1000 m a.s.l., generates layover and shadow in the SAR image and occlusion in the optical image and contributes to the high RMSE of DEMs in this interval. In Table 2, the RMSE of the original TDM DEM is the largest which is about 67 m for LVIS 2015 and 45.5 m for ATL06 2019 dataset. The surface elevation change rate between 2013 and 2016 over HG is about -3 m/a (Rott et al., 2018). The mean height difference of the original TDM DEM compared to the LVIS 2015 dataset is about 40 m for height interval below 1000 m a.s.l, which is beyond the realistic elevation surface change that could happen on HG within 1–2 years (Rott et al., 2018) and can be therefore attributed to height errors.

After the multi-scale height error correction, the height error of the TDM DEM is obviously reduced, which can be seen in terms of mean height error, root mean square error (RMSE), and quantile 90% of the height errors for different height intervals. Once again, the effectiveness of the proposed multi-scale height error correction method is validated both qualitatively and quantitatively at the individual glacier scale.

https://doi.org/10.5194/tc-2020-323
Preprint. Discussion started: 4 December 2020

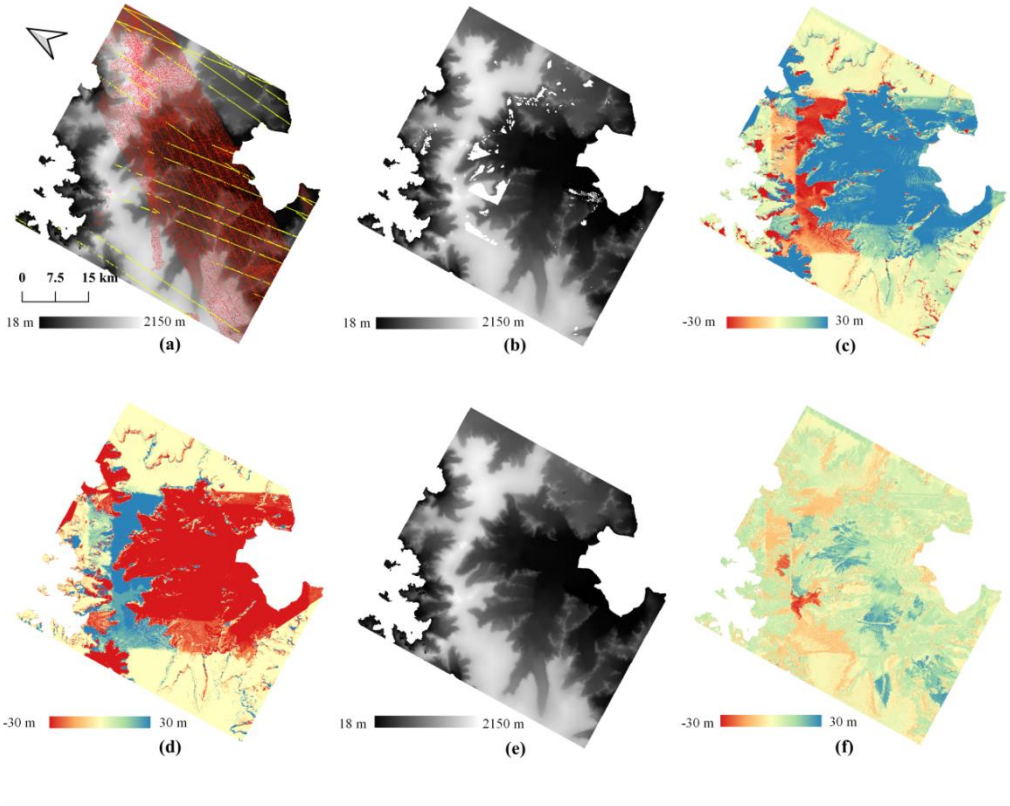

Figure 7. Experimental results of Hektoria and Green (HG) glaciers. (a) original TDM DEM. Red and yellow: the footprint of LVIS 2015 and ATL06 2019, respectively. (b) original REMA mosaic with voids. (c) elevation difference between TDM DEM and REMA mosaic. Height differences calculated as TDM DEM minus REMA mosaic. (d) correction map for TDM DEM. (e) corrected TDM DEM. (f) residual elevation difference between the corrected TDM DEM and REMA mosaic.

https://doi.org/10.5194/tc-2020-323
Preprint. Discussion started: 4 December 2020


The Cryosphere Discussions
Open Access
EGU

Table 2. Statistics of DEM height differences between the laser altimetry points and REMA mosaic, original and corrected TDM DEMs over the Hektoria and Green Glaciers area in Figure 7. All height units are in meters. Height differences calculated as DEM elevation minus laser height.

		Elevation range	Num. of points	Mean	RMSE	90% quantile
LVIS 2015	REMA mosaic	>= 15	3305813	0.6	8.7	7.0
		15-500	1420706	0.7	6.5	7.2
		500-1000	894006	0.4	9.3	7.5
		1000-1500	268063	0.9	16.8	14.0
		1500-2000	639531	0.7	7.7	2.0
		>=2000	83507	-0.6	1.5	1.0
	original TDM DEM	>= 15	3393535	29.9	42.7	65.8
		15-500	1357308	47.2	23.7	65.5
		500-1000	1020338	37.2	44.0	79.5
		1000-1500	297074	18.7	67.1	87.0
		1500-2000	639416	-9.6	29.1	9.0
		2000-2500	79399	0.8	13.7	6.0
	corrected TDM DEM	>= 15	3412552	5.0	10.5	14.5
		15-500	1439149	7.2	8.0	16.0
		500-1000	974766	4.4	11.4	13.5
		1000-1500	272005	4.7	17.4	18.0
		1500-2000	641497	1.5	9.5	10.0
		>=2000	85135	1.4	5.0	6.0
ATL06 2019	REMA mosaic	>= 15	19063	3.7	8.3	15.2
		15-500	7069	5.7	9.4	19.4
		500-1000	6590	4.8	8.7	16.5
		1000-1500	859	1.8	7.2	10.0
		1500-2000	4221	-0.5	2.8	2.0
		>=2000	324	-1.7	1.1	0.0
	original TDM DEM	>= 15	20401	25.5	34.2	73.3
		15-500	7780	47.7	28.5	79.0
		500-1000	7076	23.8	27.0	67.0
		1000-1500	871	11.6	45.5	24.0
		1500-2000	4347	-7.0	19.8	4.0
		>=2000	327	1.0	4.9	4.4
	corrected TDM DEM	>= 15	20507	8.7	12.87	25.8
		15-500	8081	14.7	14.5	34.0
		500-1000	6856	8.7	10.2	18.0
		1000-1500	872	3.5	7.6	10.9
		1500-2000	4372	-0.9	6.6	5.0
		>=2000	326	1.2	3.2	4.0

https://doi.org/10.5194/tc-2020-323
Preprint. Discussion started: 4 December 2020

4.3 Experimental results on Antarctic Peninsula

The multi-scale height errors correction was also applied to entire Antarctic Peninsula north of 70 ° S (Fig. 8 left) covering about 95 000 km^2. Because the corrections are not visible over such a large area, we show the results on the detailed views of three sample areas marked as A, B and C (Fig. 8a and Fig. 8b). Within each area, the corrected elevations become smooth and continuous with elevation jumps successfully eliminated.

The corrected TDM DEM was evaluated with the LVIS 2015 and ATL06 2019 datasets covering entire AP according to the footprints shown in Figure 1. The statistics of the DEM height errors at the laser points are presented in Table 3. For the original TDM DEM, the average RMSE at all elevations is about 27 m with LVIS 2015 dataset and about 20 m with ATL06 2019 dataset. After the multi-scale correction, the RMSE of the corrected TDM DEM reduces to 12 m with all the laser points. The large-scale elevation errors of TDM DEM mainly happen below 500 m a.s.l. where the 90% quantile of height errors of original TDM DEM can reach 50 m with LVIS 2015 dataset and is reduced to about 10 m after the correction. For the ATL06 dataset, the RMSE and 90% quantile of height errors remain stable before and after the correction for height interval below 500 m a.s.l., which is because the number of the ATL06 laser points is much smaller than that of the LVIS 2015 dataset and the existing ATL 06 laser points happen to locate at the regions with limited residual height errors. At the plateaus above 2000 m, the original TDM DEM has high height measurement accuracy and does not change much after the correction.

https://doi.org/10.5194/tc-2020-323
Preprint. Discussion started: 4 December 2020

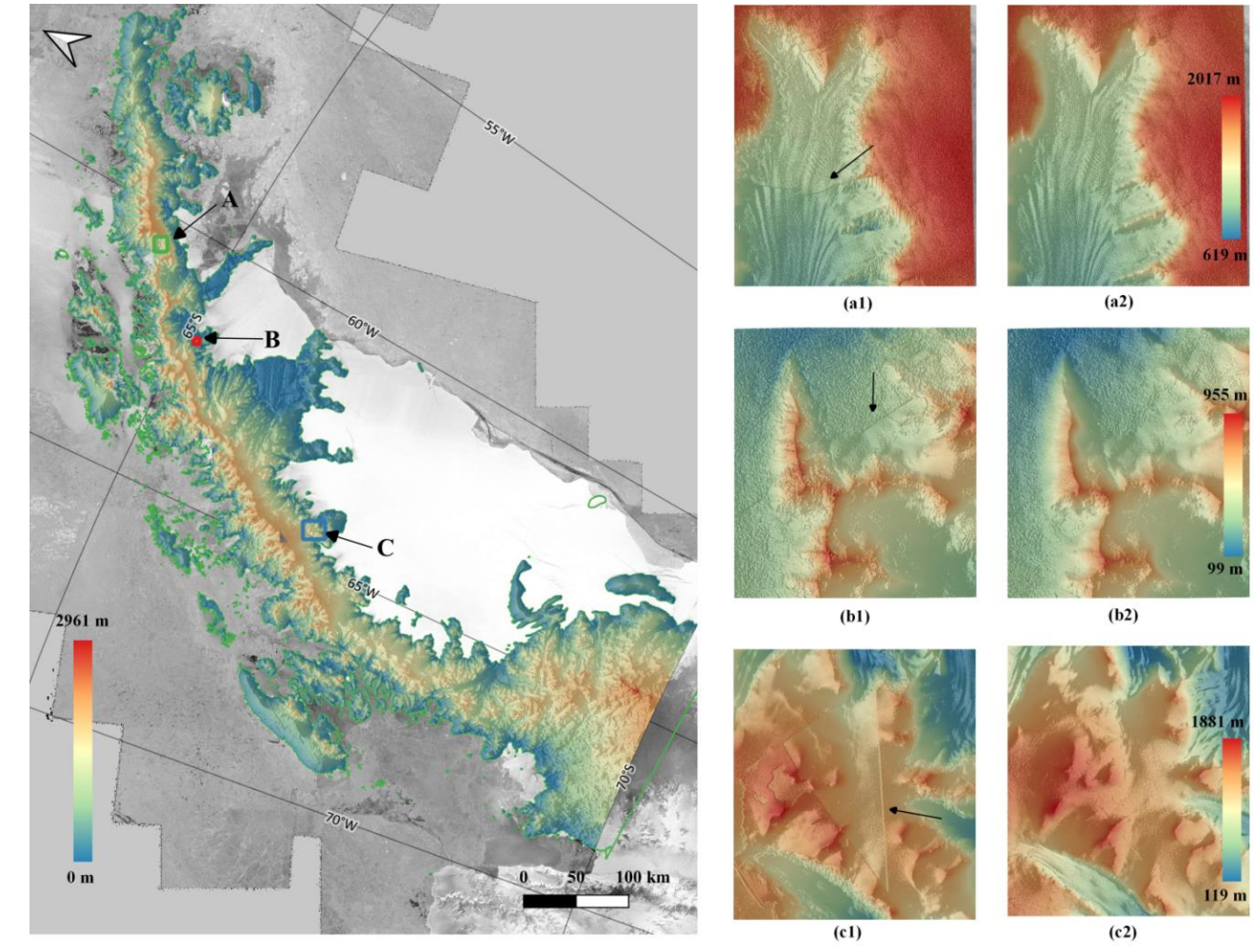

Fig. 8. Left: Corrected TDM DEM of the Antarctic Peninsula and the location of the sample areas. Right: comparison of original TDM DEM (a) with the corrected TDM DEM (b) at the sample areas A, B and C. Black arrows point to the boundaries of the erroneous areas which have to be eliminated.

https://doi.org/10.5194/tc-2020-323
Preprint. Discussion started: 4 December 2020

The Cryosphere Discussions
Open Access
EGU

Table 3. Statistics of DEM height differences between the laser points and the REMA mosaic, original and corrected TDM DEMs over Antarctic Peninsula in Fig. 8. All height units are in meters. Height differences calculated as DEM elevation minus laser height.

		Elevation range	Num. of points	Mean	RMSE	90% quantile
LVIS 2015	REMA mosaic	>= 15	31764790	1.1	11.6	5.0
		15-500	8666409	0.8	11.7	4.3
		500-1000	7328037	1.1	16.5	6.0
		1000-1500	7776100	1.4	10.5	6.0
		1500-2000	7332887	1.2	5.4	4.0
		>=2000	661357	1.5	5.3	4.0
	original TDM DEM	>= 15	33246648	3.4	26.8	10.8
		15-500	8780391	9.0	26.5	50.2
		500-1000	7646140	5.6	32.8	17.0
		1000-1500	8387426	0.2	26.0	6.0
		1500-2000	7696065	-1.5	20.3	6.0
		>=2000	736626	2.2	9.0	7.0
	corrected TDM DEM	>= 15	33342330	2.4	12.9	8.0
		15-500	8846764	3.9	12.1	10.3
		500-1000	7613741	3.2	16.9	9.5
		1000-1500	8363164	1.2	13.6	6.0
		1500-2000	7771157	1.4	7.9	6.0
		>=2000	747504	1.7	7.8	7.0
ATL06 2019	REMA mosaic	>= 15	921748	0.6	6.3	4.5
		15-500	296629	1.4	6.9	6.8
		500-1000	202191	0.5	8.2	6.0
		1000-1500	165822	0.3	6.2	4.0
		1500-2000	221045	0.0	3.1	3.0
		>=2000	36061	0.6	2.2	2.0
	original TDM DEM	>= 15	980500	-0.1	19.6	6.0
		15-500	314037	3.6	12.9	9.0
		500-1000	214729	1.1	17.9	7.5
		1000-1500	180578	-3.3	24.8	3.0
		1500-2000	234570	-3.6	23.8	4.0
		>=2000	36586	-0.6	8.1	4.0
	corrected TDM DEM	>= 15	981642	0.7	11.6	6.0
		15-500	314064	2.1	13.6	8.5
		500-1000	214425	1.7	9.2	7.0
		1000-1500	180266	-1.0	14.1	3.0
		1500-2000	235679	-0.5	8.1	4.0
		>=2000	37208	-0.9	6.7	4.0

https://doi.org/10.5194/tc-2020-323
Preprint. Discussion started: 4 December 2020

5 Discussion

5.1 The effectiveness of the proposed method for the different height error patterns

The results presented in Section 4 demonstrate the effective elimination the residual height errors in the TDM DEM product through validation with the high-precision laser altimetry data (Table 1–Table 3). Examples of residual height errors in the TDM DEM product were visualized in the height difference maps (Figure 6c and Figure 7c). In this section, the height errors in the TDM DEM are analysed along several elevation profiles (positioned as in Figure 9a and Figure 10a) extracted from the TDM DEM before and after correction. We preserved the experimental areas used in Sections 4.1 and 4.2. From the profiles in Figure 9 and Figure 10b–Figure 10e the erroneous heights can be roughly divided into two patterns. Their influence on the effectiveness of the proposed method will be evaluated qualitatively below.

In Figure 9, the profile can be divided into sub-segments with similar offsets ranging from tens to hundreds of meters. Also, along the profiles L3 and L4 spatially-connected points deviate from the correct height values with a certain offset (Figure 10d and Figure 10e). These jumps are much larger than the height difference between TDM DEM and REMA mosaic and cannot be caused by the X-band microwave penetration depth (from several meters to 10 m for high penetration conditions) (Rizzoli et al., 2017b) or temporal surface height changes (-3 m/a at HG between 2013 and 2016) (Rott et al., 2018). Besides, the clear boundary in the DEM hillshade map (Figure 9a) and the height jumps in the height profiles (Figure 9 and Figure 10b–Figure 10e) further confirm the existence of the residual height errors and exclude the influence of signal penetration and temporal height surface changes. This kind of local height offsets are typical height errors introduced from phase unwrapping errors due to erroneous determination of phase ambiguity. The path propagation method described in Section 3.2 can automatically detect the local regions affected by height offsets and segment them into sub-regions with similar offset. The proposed correction method in Section 3.3 takes the offsets between TDM DEM and REMA mosaic at stable areas around the erroneous region into consideration, thus avoiding over-correcting the TDM DEM to the REMA mosaic. As a result, the corrected height profiles are continuous and smooth (black lines in Figure 9 and Figure 10b–Figure 10e) and the spatial details are well preserved even after eliminating the abnormal offset e.g. as along profile L4 (Figure 10e).

Unlike the local continuous region with similar height offsets, profile L1 (Figure 10b) shows the height inconsistency pattern when the erroneous region neither has a unified elevation offset like L3 (Figure 10d) and L4 (Figure 10e) nor can be segmented into sub-regions with similar offset and clear boundary as in Figure 9. The regional elevation offsets in Figure 10b are still related to phase unwrapping errors. However, the scene-based weighted average processing when generating the final TDM global DEM mosaic make it difficult to distinguish the original PU errors in the raw DEMs. In addition, the residual calibration error may introduce near a vertical offset and a horizontal tilt (and shift), thus contributing to the elevation inconsistency in the final TDM DEM. Under these circumstances, the height correction depends on the detected erroneous regions from path propagation algorithm and is more influenced by the REMA DEM. Another case is shown for profile L2 (Figure 10c) where elevation anomalies with smaller spatial size occur. L2 can be seen as a combination of different patterns where the proposed correction method can also work effectively by removing height offsets and noise

https://doi.org/10.5194/tc-2020-323
Preprint. Discussion started: 4 December 2020

(Figure 10c).

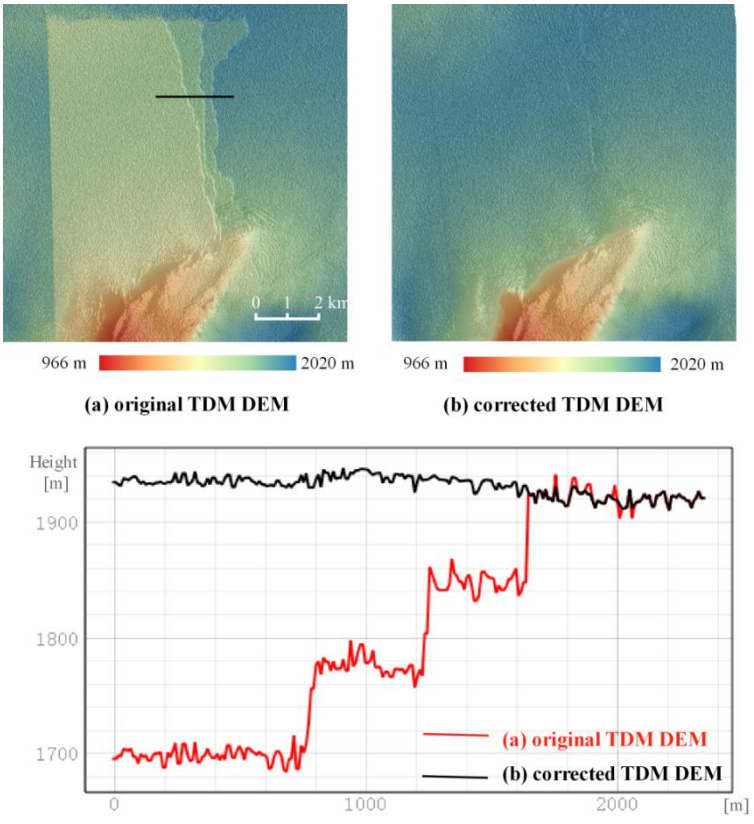

365

Figure 9. Height profiles along the black line extracted from (a) original and (b) corrected TDM DEM of local sample area.

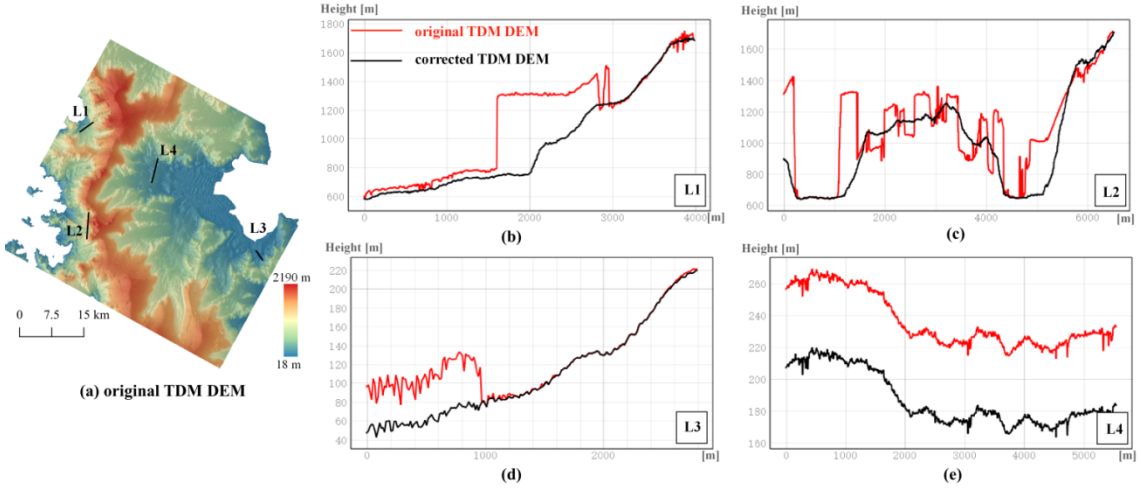

Figure 10. Four height profiles extracted along lines L1-L4 from original and corrected TDM DEM at HG area.

https://doi.org/10.5194/tc-2020-323
Preprint. Discussion started: 4 December 2020

370 **5.2 The importance of multi-scale height error correction strategy**

Taking into consideration the various vertical scales of the residual height errors we have proposed the multi-scale height error correction method in Section 3.4. Here we discuss the necessity of the multi-scale height errors correction strategy as well as the validation methods.

In our experiments, we performed three corrections to correct the large-scale errors (> 45 m), medium-scale height errors (> 375 20 m) and the small-scale height errors (> 10 m). The intermediate results after each correction are shown on the local and HG area in Figure 11 and Figure 12 and the corresponding elevation differences when compared to LVIS 2015 and ATL06 2019 data are given in Table S2 and Table S3 in the supplementary material. The magnitude of the height differences could be reduced gradually after each correction step as obvious from the decreasing elevation range in the difference maps. Table S2 and Table S3 show also how the mean values of height errors get closer to zero and the RMSEs are reduced. The third 380 correction barely changes the mean value but slightly reduces the RMSE, which plays the role of de-noising the DEM.

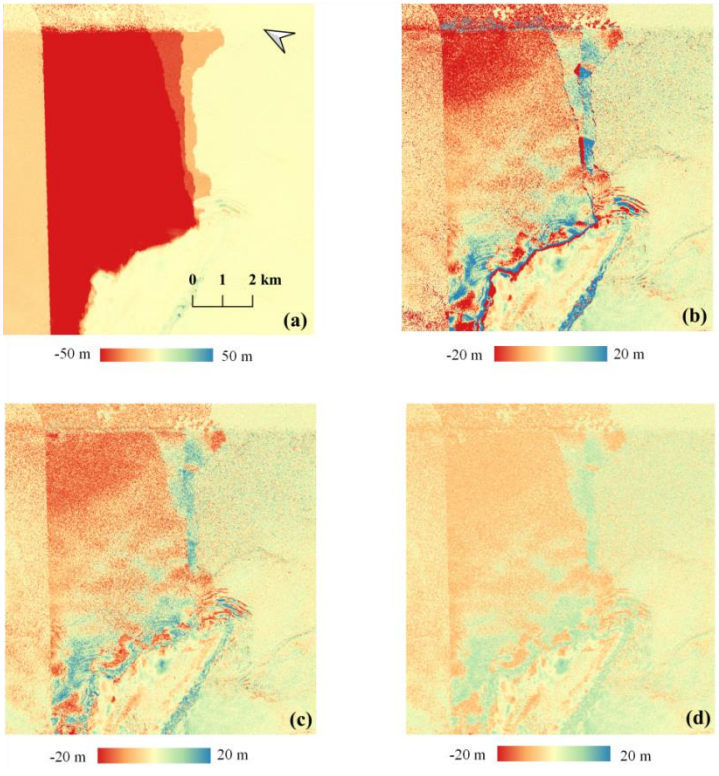

Figure 11. Height difference maps of the local area between (a) original TDM DEM, (b) TDM DEM after 1st, (c) TDM DEM after 2nd, (d) TDM DEM after 3rd multi-scale correction and REMA mosaic. Height differences calculated as TDM DEM minus REMA mosaic.

https://doi.org/10.5194/tc-2020-323
Preprint. Discussion started: 4 December 2020

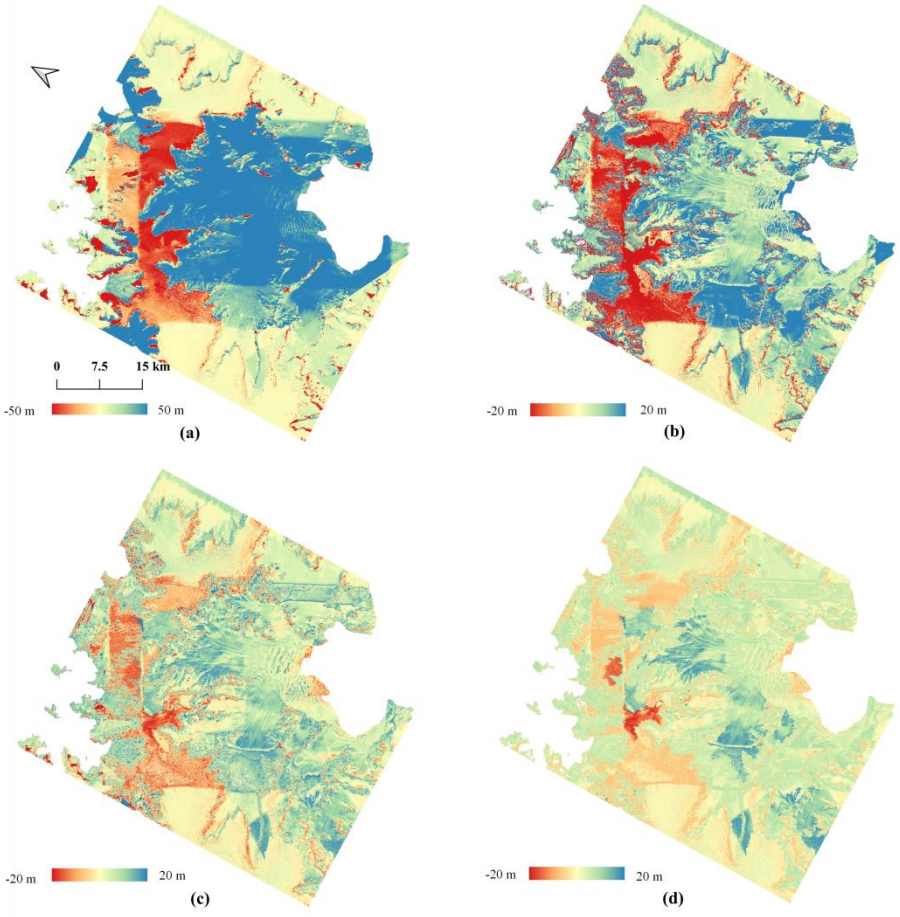

385 **Figure 12.** Height difference maps of HG area between (a) original TDM DEM, (b) TDM DEM after 1st correction, (c) TDM DEM after 2nd correction, (d) TDM DEM after 3rd correction and the REMA mosaic. Height differences calculated as TDM DEM minus REMA mosaic.

6 Conclusions

In order to meet the high-resolution topography data demand of fine-scale glaciological research, we combined elevation
390 information provided by two up-to-date large scale high-resolution DEM products, the 12-m TanDEM-X DEM (TDM DEM) and the 8-m REMA mosaic, to generate a high-resolution precise consistent and gapless DEM of AP. Prior to the combination with REMA, the TDM DEM is characterized by good data consistency and few data voids, but contains residual systematic height errors introduced by baseline calibration, geometric distortion and phase unwrapping. The REMA mosaic has advantageous, high absolute vertical accuracy (about 1 m) and absence of regional outliers. Combining the
395 advantages of TDM DEM and REMA mosaic, we identified the areas in the TDM DEM affected by errors with a path

https://doi.org/10.5194/tc-2020-323
Preprint. Discussion started: 4 December 2020

propagation algorithm and developed the multi-scale method to automatically correct the height errors in the TDM DEM. The effectiveness of the proposed method and the vertical accuracy of the resulting DEM were validated by visual inspection and laser altimetry data. The main findings of our research are as follows:

1) The path propagation algorithm can effectively detect erroneous regions with similar height offsets which include the remaining phase unwrapping errors in TDM DEM based on different offsets of neighboring regions. The path propagation algorithm aims at merging the adjacent homogeneous pixels into one region and is stopped at background pixels and heterogeneous pixels, which allows a successful detection of regions with different height offsets even with blurry boundaries.

2) The height offset compensation with a fitted reference surface from selected stable points can maintain the reference height surface of the TDM DEM. The height difference between TDM DEM and REMA mosaic caused by the penetration depth of TDM DEM and temporal surface change should be excluded from the height error in TDM DEM. Therefore we created buffer zones around each extracted erroneous region and selected stable points to create a reference surface around the erroneous region to calculate the compensation height value. In other words, we take advantage of the spatial constraint information to avoid over-correction.

3) The multi-scale method can comprehensively correct the height errors in TDM DEM by iteratively adjusting the height errors with different height scale. TDM DEM is superior in data consistency and completeness. The proposed multi-scale correction maintains the elevation surface of the TDM DEM and eliminates the residual height errors especially the phase unwrapping error. Inevitably, the corrected TDM DEM is influenced by the REMA DEM especially when there is a superposition of phase unwrapping and calibration errors due to the scene-based weighted average processing applied to generate the final TDM DEM product.

In general, the DEM over AP resulting from the combination of TanDEM-X DEM and REMA mosaic maintains the characteristics of the TanDEM-X DEM and has a better quality due to the correction of the residual height errors. Due to its consistency, spatial continuity, high-resolution and accuracy it is beneficial to use the resulting corrected DEM in various glaciological applications requiring detailed gapless topography information. In interferometric SAR processing the presented DEM can support the modelling of the topographic phase when separating this contribution from displacements and vertical deformation. DEM time series needed for the geodetic mass balance can be precisely vertically co-registered using our DEM as reference surface. Also drainage basin delineations of individual glaciers rely on accurate DEMs. The proposed method can be extended to other areas of the Antarctic Ice Sheet where SAR and optical DEMs are prone to errors like mountainous coastal regions or in the Transantarctic Mountains.

Data availability. The improved DEM dataset will be made available upon publication of the final version via the EOC Geoservice of the Earth Observation Center (EOC) of the German Aerospace Center (DLR) (https://geoservice.dlr.de/web/).

Competing interests. The authors declare that they have no competing interests.

https://doi.org/10.5194/tc-2020-323
Preprint. Discussion started: 4 December 2020

References

Abdel Jaber, W., Rott, H., Floricioiu, D., Wuite, J., and Miranda, N.: Heterogeneous spatial and temporal pattern of surface elevation change and mass balance of the Patagonian ice fields between 2000 and 2016, The Cryosphere, 13, 2511-2535, 2019.

Abrams, M., Crippen, R., and Fujisada, H.: ASTER Global Digital Elevation Model (GDEM) and ASTER Global Water Body Dataset (ASTWBD), Remote Sens., 12, 1156, 2020.

ASTER GDEM Validation Team: ASTER Global Digital Elevation Model Version 2 – Summary of Validation Results, NASA Land Processes Distributed Active Archive Center and Joint Japan-US ASTER Science Team, available at: http://www.jspacesystems.or.jp/ersdac/GDEM/ver2Validation/Summary GDEM2 validation report final.pdf, 2011, 2009.

ASTER GDEM Validation Team: METI/ERSDAC, NASA/LPDAAC, USGS/EROS, in cooperation with NGA and other collaborators, ASTER GDEM Validation Summary Report, available at: http://www.jspacesystems.or.jp/ersdac/GDEM/E/image/ASTERGDEM ValidationSummaryReport Ver1.pdf, 2009, 2011.

Bamber, J., Gomez-Dans, J., and Griggs, J.: A new 1 km digital elevation model of the Antarctic derived from combined satellite radar and laser data–Part 1: Data and methods, The Cryosphere, 3, 101-111, 2009.

Brunt, K., Neumann, T., and Smith, B.: Assessment of ICESat-2 Ice Sheet Surface Heights, Based on Comparisons Over the Interior of the Antarctic Ice Sheet, Geophys. Res. Lett., 46, 13072-13078, 2019.

Cook, A., Fox, A., Vaughan, D., and Ferrigno, J.: Retreating glacier fronts on the Antarctic Peninsula over the past half-century, Science, 308, 541-544, 2005.

Cook, A. J., Murray, T., Luckman, A., Vaughan, D. G., and Barrand, N. E.: A new 100-m Digital Elevation Model of the Antarctic Peninsula derived from ASTER Global DEM: methods and accuracy assessment, Earth system science data., 4, 129-142, 2012.

Cook, A. J., Vaughan, D. G., Luckman, A. J., and Murray, T.: A new Antarctic Peninsula glacier basin inventory and observed area changes since the 1940s, Antarct. Sci., 26, 614-624, 10.1017/S0954102014000200, 2014.

Cook, A. J., Holland, P., Meredith, M., Murray, T., Luckman, A., and Vaughan, D. G.: Ocean forcing of glacier retreat in the western Antarctic Peninsula, Science, 353, 283-286, 2016.

Cornford, S. L., Martin, D. F., Payne, A., Ng, E., Le Brocq, A., Gladstone, R., Edwards, T. L., Shannon, S., Agosta, C., and Van Den Broeke, M.: Century-scale simulations of the response of the West Antarctic Ice Sheet to a warming climate, The Cryosphere, 9, 1579-1600, 2015.

DiMarzio, J., Brenner, A., Schutz, R., Shuman, C., and Zwally, H.: GLAS/ICESat 500 m laser altimetry digital elevation model of Antarctica, National Snow and Ice Data Center, 2007.

Dryak, M. C., and Enderlin, E. M.: Analysis of Antarctic Peninsula glacier frontal ablation rates with respect to iceberg melt-inferred variability in ocean conditions, J. Glaciol., 66, 457-470, 10.1017/jog.2020.21, 2020.

Fretwell, P., Pritchard, H. D., Vaughan, D. G., Bamber, J. L., Barrand, N., Bell, R., Bianchi, C., Bingham, R., Blankenship, D. D., and Casassa, G.: Bedmap2: improved ice bed, surface and thickness datasets for Antarctica, The Cryosphere, 7, 375-393, 2013.

German Aerospace Center DLR: Digital Elevation Model (DEM) - Global, 90m. https://doi.org/10.15489/ju28hc7pui09, 2018.

González, J. H., Antony, J. M. W., Bachmann, M., Krieger, G., Zink, M., Schrank, D., and Schwerdt, M.: Bistatic system and baseline calibration in TanDEM-X to ensure the global digital elevation model quality, ISPRS J. Photogramm. Remote Sens., 73, 3-11, 2012.

Griggs, J., and Bamber, J.: A new 1 km digital elevation model of Antarctica derived from combined radar and laser data-Part 2: Validation and error estimates, The Cryosphere, 3, 113, 2009.

Gruber, A., Wessel, B., Huber, M., and Roth, A.: Operational TanDEM-X DEM calibration and first validation results, ISPRS J. Photogramm. Remote Sens., 73, 39-49, 2012.

Gruber, A., Wessel, B., Martone, M., and Roth, A.: The TanDEM-X DEM Mosaicking: Fusion of Multiple Acquisitions Using InSAR Quality Parameters, IEEE J. Sel. Topics Appl. Earth Observ. Remote Sens., 9, 1047-1057, 10.1109/jstars.2015.2421879, 2016.

Helm, V., Humbert, A., and Miller, H.: Elevation and elevation change of Greenland and Antarctica derived from CryoSat-2, The Cryosphere, 8, 1539-1559, 2014.

Hofton, M., Blair, J., Luthcke, S., and Rabine, D.: Assessing the performance of 20–25 m footprint waveform lidar data collected in

https://doi.org/10.5194/tc-2020-323
Preprint. Discussion started: 4 December 2020

ICESat data corridors in Greenland, Geophys. Res. Lett., 35, 2008.

Howat, I. M., Porter, C., Smith, B. E., Noh, M.-J., and Morin, P.: The reference elevation model of Antarctica, The Cryosphere, 13, 665-674, 2019.

Huber, J., Cook, A. J., Paul, F., and Zemp, M.: A complete glacier inventory of the Antarctic Peninsula based on Landsat 7 images from 2000 to 2002 and other preexisting data sets, Earth system science data., 9, 115-131, 2017.

Huss, M., and Farinotti, D.: A high-resolution bedrock map for the Antarctic Peninsula, The Cryosphere, 8, 1261-1273, 2014.

Korona, J., Berthier, E., Bernard, M., Rémy, F., and Thouvenot, E.: SPIRIT. SPOT 5 stereoscopic survey of polar ice: reference images and topographies during the fourth International Polar Year (2007–2009), ISPRS J. Photogramm. Remote Sens., 64, 204-212, 2009.

Krieger, G., Moreira, A., Fiedler, H., Hajnsek, I., Werner, M., Younis, M., and Zink, M.: TanDEM-X: A satellite formation for high-resolution SAR interferometry, IEEE Trans. Geosci. Remote Sens., 45, 3317-3341, 2007.

Krieger, G., Zink, M., Bachmann, M., Bräutigam, B., Schulze, D., Martone, M., Rizzoli, P., Steinbrecher, U., Antony, J. W., and De Zan, F.: TanDEM-X: A radar interferometer with two formation-flying satellites, Acta Astronaut., 89, 83-98, 2013.

Krieger, L., Floricioiu, D., and Neckel, N.: Drainage basin delineation for outlet glaciers of Northeast Greenland based on Sentinel-1 ice velocities and TanDEM-X elevations, Remote Sens. Environ., 237, 111483, 2020a.

Krieger, L., Ströße nreuther, U., Helm, V., Floricioiu, D., and Horwath, M.: Synergistic Use of Single-Pass Interferometry and Radar Altimetry to Measure Mass Loss of NEGIS Outlet Glaciers between 2011 and 2014, Remote Sens., 12, 996, 2020b.

Lachaise, M., Fritz, T., and Bamler, R.: The dual-baseline phase unwrapping correction framework for the TanDEM-X mission part 1: Theoretical description and algorithms, IEEE Trans. Geosci. Remote Sens., 56, 780-798, 2017.

Li, F., Xiao, F., Zhang, S. K., E, D. C., Cheng, X., Hao, W. F., Yuan, L. X., and Zuo, Y. W.: DEM development and precision analysis for Antarctic ice sheet using Cryosat-2 altimetry data, Chin. J. Geophys., 60, 231-243, 2017.

Liu, H., Jezek, K., Li, B., and Zhao, Z.: Radarsat Antarctic Mapping Project digital elevation model version 2, Digital media, National Snow and Ice Data Center, Boulder, CO, USA, 2001.

Mouginot, J., Scheuchl, B., and Rignot, E.: Mapping of ice motion in Antarctica using synthetic-aperture radar data, Remote Sens., 4, 2753-2767, 2012.

Rignot, E., Mouginot, J., and Scheuchl, B.: Ice flow of the Antarctic ice sheet, Science, 333, 1427-1430, 2011a.

Rignot, E., Velicogna, I., van den Broeke, M. R., Monaghan, A., and Lenaerts, J. T.: Acceleration of the contribution of the Greenland and Antarctic ice sheets to sea level rise, Geophys. Res. Lett., 38, 2011b.

Rignot, E., Mouginot, J., Scheuchl, B., van den Broeke, M., van Wessem, M. J., and Morlighem, M.: Four decades of Antarctic Ice Sheet mass balance from 1979–2017, Proc. Natl. Acad. Sci. U.S.A., 116, 1095-1103, 2019.

Ritz, C., Edwards, T. L., Durand, G., Payne, A. J., Peyaud, V., and Hindmarsh, R. C.: Potential sea-level rise from Antarctic ice-sheet instability constrained by observations, Nature, 528, 115-118, 2015.

Rizzoli, P., Bräutigam, B., Kraus, T., Martone, M., and Krieger, G.: Relative height error analysis of TanDEM-X elevation data, ISPRS J. Photogramm. Remote Sens., 73, 30-38, http://dx.doi.org/10.1016/j.isprsjprs.2012.06.004, 2012.

Rizzoli, P., Martone, M., Gonzalez, C., Wecklich, C., Tridon, D. B., Bräutigam, B., Bachmann, M., Schulze, D., Fritz, T., and Huber, M.: Generation and performance assessment of the global TanDEM-X digital elevation model, ISPRS J. Photogramm. Remote Sens., 132, 119-139, 2017a.

Rizzoli, P., Martone, M., Rott, H., and Moreira, A.: Characterization of snow facies on the Greenland ice sheet observed by TanDEM-X interferometric SAR data, Remote Sens., 9, 315, 2017b.

Rott, H., Abdel Jaber, W., Wuite, J., Scheiblauer, S., Floricioiu, D., Van Wessem, J. M., Nagler, T., Miranda, N., and Van Den Broeke, M. R.: Changing pattern of ice flow and mass balance for glaciers discharging into the Larsen A and B embayments, Antarctic Peninsula, 2011 to 2016, Cryosphere, 12, 1273-1291, 2018.

Seehaus, T., Cook, A. J., Silva, A. B., and Braun, M.: Changes in glacier dynamics in the northern Antarctic Peninsula since 1985, The Cryosphere, 12, 577-594, 2018.

Shepherd, A., Ivins, E., Rignot, E., Smith, B., Van Den Broeke, M., Velicogna, I., Whitehouse, P., Briggs, K., Joughin, I., and Krinner, G.: Mass balance of the Antarctic Ice Sheet from 1992 to 2017, Nature, 558, 219-222, 2018.

https://doi.org/10.5194/tc-2020-323
Preprint. Discussion started: 4 December 2020

Slater, T., Shepherd, A., McMillan, M., Muir, A., Gilbert, L., Hogg, A. E., Konrad, H., and Parrinello, T.: A new digital elevation model of Antarctica derived from CryoSat-2 altimetry, The Cryosphere, 12, 1551-1562, 2018.

520 Sutterley, T. C., Velicogna, I., Rignot, E., Mouginot, J., Flament, T., Van Den Broeke, M. R., Van Wessem, J. M., and Reijmer, C. H.: Mass loss of the Amundsen Sea Embayment of West Antarctica from four independent techniques, Geophys. Res. Lett., 41, 8421-8428, 2014.